crystals

MDPI

Synthesis, Single Crystal X-Ray Analysis, Prediction and Study of Pharmacological Activity of 4-(1*H*-Benzo[d]imidazol-2-yl)-1-Phenyl-1*H*-1,2,3-triazol-5-Amine and Its Solvates

Alexandre V. Ivachtchenko [1], Oleg D. Mitkin [1,*], Dmitry V. Kravchenko [2],
Sergiy M. Kovalenko [1,3,6], Svitlana V. Shishkina [3,5,6], Natalya D. Bunyatyan [3,4],
Irina S. Konovalova [5], Vladimir V. Ivanov [6], Olena D. Konovalova [6] and Thierry Langer [7]

[1]   ChemRar Research and Development Institute, Innovation Center Skolkovo territory, 7 Nobel st.,
      Moscow 143026, Russia; av@chemrar.ru (A.V.I.); kovalenko.sergiy.m@gmail.com (S.M.K.)
[2]   Chemical Diversity Research Institute, 2A Rabochaya st., Khimki, Moscow Region 141400, Russia;
      dk@chemrar.ru
[3]   Sechenov First Moscow State Medical University of the Ministry of Healthcare of the Russian
      Federation (Sechenov University), 8 Trubeckaya st., Moscow 119991, Russia;
      sveta@xray.isc.kharkov.com (S.V.S.); ndbun@mail.ru (N.D.B.)
[4]   Federal State Budgetary Institution "Scientific Centre for Expert Evaluation of Medicinal Products" of the
      Ministry of Health of the Russian Federation, Petrovsky boulevard 8, bld. 2, Moscow 127051, Russia
[5]   State Scientific Institution "Institute for Single Crystals" of the National Academy of Sciences of Ukraine,
      61001 Kharkov, Ukraine; ikonovalova0210@gmail.com
[6]   V.N.Karazin Kharkiv National University, 4 Svobody sq., 61077 Kharkiv, Ukraine;
      vivanov@univer.kharkov.ua (V.V.I.); valeolog@karazin.ua(O.D.K.)
[7]   Department of Pharmaceutical Chemistry, University of Vienna, Althanstraße 14, A-1090 Vienna, Austria;
      thierry.langer@univie.ac.at
*   Correspondence: mod@chemrar.ru; Tel.: +7-495-995-4941

check for updates

Abstract: A method for the synthesis of 4- (1*H*-benzo[d]imidazole-2-yl)-1-phenyl-1*H*-1,2,3-triazole-5-amine was developed, and the electronic and spatial structure of this molecule was studied theoretically and experimentally. The study of interaction energies between molecules by quantum-chemical calculations allows us to recognize different levels of crystal structure organization and describe the interaction types causing their formation. The classic N-H . . . N and C-H . . . N hydrogen bonds play the main role in all the studied crystals forming the primary basic structural motif. Their role is comparable with the role of the stacking interactions. The molecular docking study predicted that the studied compound may exhibit anti-hepatitis B activity, and experimental in vitro studies confirmed that it is a potent HBV inhibitor with IC_{50} in a low micromolar range.

1. Introduction

Nitrogen-containing heterocycles are especially considered "privileged" structures for the synthesis and development of new drugs [1–3]. Among them, benzimidazole and its derivatives have a significant role due to their wide variety of pharmacological properties [4] such as anticancer [5], antitumor [6], anti-inflammatory [7], anti-diabetic [8], antimalarial [9], antimicrobial [10] and antifungal activity [11]. Triazoles are shown to possess a wide spectrum of interesting biological activities

including anti-allergic [12], anti-HIV and anti-hepatitis C [13–15], anti-inflammatory [16], antifungal [17], anti-tubercular [18,19], and antimicrobial [20]. Some of them have also shown significant anticancer activity in many human cell lines [21].

One of the promising areas of pharmaceutical chemistry is the creation of dipharmacophore substances incorporating molecular groups of various therapeutic orientations. This approach allows us to design new biologically active substances that have innovative potentials. A number of papers describe dipharmacophore molecules containing in their structures covalently linked 1,2,3-triazolide and benzimidazole moieties [22–24].

In the present work, using 4-(1*H*-benzo[d]imidazol-2-yl)-1-phenyl-1*H*-1,2,3-triazol-5-amine as an example, we developed a one-step method for the synthesis of benzimidazole–1,2,3-triazole hybrid molecules. We studied its electronic and crystal structure using spectral methods and X-ray diffraction analysis. Based on the results of 3D pharmacophore screening, we also evaluated the potential pharmacological activity of this molecule as well as its solvated forms.

2. Results and Discussion

The initial structure of the studied "benzimidazole – 1,2,3-triazole" dual moiety molecules, 4-(1*H*-benzo[d]imidazol-2-yl)-1-phenyl-1*H*-1,2,3-triazol-5-amine **3**, has not yet been described in the literature. There is only information on the synthesis of its 4-nitro- and 4-bromo-derivatives [25]. We synthesized the title compound **3** and studied it using UV-, IR-, ^{1}H NMR, and ^{13}C NMR spectroscopy (Supplementary Materials, Figures S1–S4) as well as LC/MS data for structural determination (Figure S5). Finally, the structure of the title compound was confirmed by X-ray analysis (Figure 1).
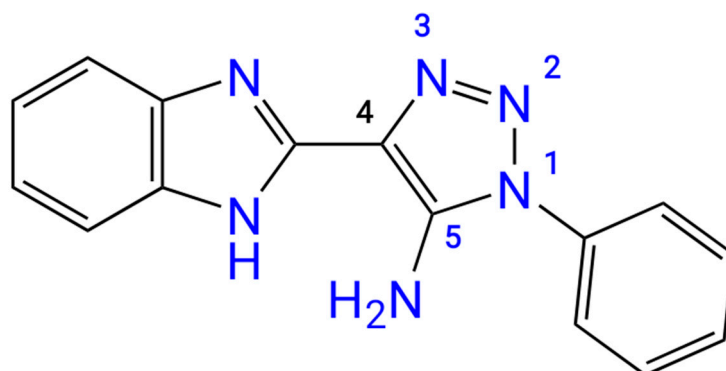

Figure 1. Chemical structure of the title compound **3**.

2.1. Synthesis and Crystallization

Compound **3** was synthesized by base-promoted (MeONa) cyclization of 2-(1*H*-benzo[d]imidazol-2-yl)acetonitrile **2** with azidobenzene **1** in methanol (Scheme 1). Depending on the solvent used for recrystallization, different solvated forms of compound **3** could also be obtained. Specifically, compounds **3a** and **3b** were obtained as solvates of **3** with THF and pyridine, respectively, at the stoichiometric ratio 1 : 1.
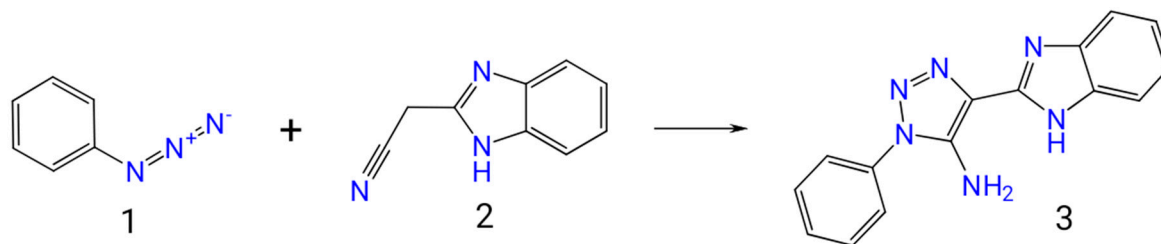
Scheme 1. Synthesis of the title compound **3**.

2.2. Molecular and Crystal Structure Analysis

The structures of compounds **3**, **3a** and **3b** were studied using different spectral methods (see Materials and Methods section, and Supplementary Materials) and finally confirmed using the single crystal X-ray diffraction analysis.

The crystallographic information and refinement data are presented in the Materials and Methods Section.

The compounds **3a** and **3b** have been obtained as solvates with THF and pyridine, respectively, at the stoichiometric ratio 1:1. The asymmetric part of the unit cell of the studied crystals contains one molecule of the title compounds (Figure 2). The bond lengths are very similar in all basic molecules of the title compounds (Table S1). The nitrogen atom of the amino group has a pyramidal configuration with different degrees of pyramidality in compounds **3**, **3a** and **3b** (Table 1). The highest degree of pyramidality is observed in crystal **3**, while the nitrogen atoms of amino group in crystals **3a** and **3b** have a smaller degree of pyramidality. This reflects considerable conjugation between the π-system of the triazole ring and the N6 atom lone pair which is confirmed by the shorter length of the C9–N6 bond (Table 1). It is caused by full involvement of two hydrogen atoms of amino group in formation of both intramolecular N6-H6NB . . . N1 and intermolecular hydrogen bonds with solvent molecules (Table 2). The phenyl substituent is turned relative to the C9–N5 endocyclic bond (the C9–N5–C10–C15 torsion angles are shown in Table 1) due to steric repulsion between vicinal substituents (the shortened intramolecular contacts are: H15 . . . N6 2.55 Å (van der Waals radii sum [26] is 2.66 Å) (**3**), H6A . . . C10 2.74 Å (2.87 Å) (**3a**), N6 . . . C15 3.16 Å (3.21 Å) (**3b**)).
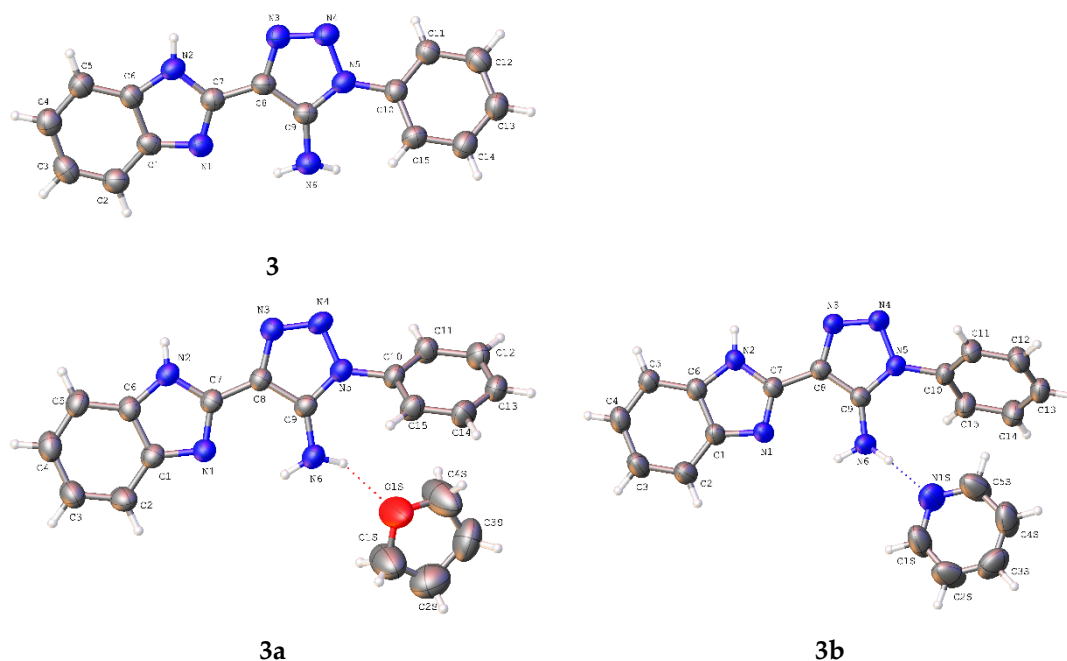

3

3a

3b

Figure 2. The molecular structure of the title compounds **3**, **3a**, **3b** showing the atom labeling scheme. Displacement ellipsoids are presented at the 50% probability level.

Table 1. Some geometrical parameters of the title compounds **3**, **3a**, **3b**.

Parameter	3	3a	3b
Bond N6-C9, Å	1.368(3)	1.356(4)	1.349(4)
Torsion angle C9-N5-C10-C15, deg	−27.1(5)	46.8(4)	48.1(5)
ΣN6, deg	339	354	354

The organic molecules such as the studied compound **3** have the ability to form solvates with different molecules which contain strong enough proton acceptors. Therefore, special attention should be paid to the intermolecular interactions and their role in the crystal structure formation.

In the crystals **3a** and **3b**, cavities that contain solvent molecules are formed. The cavities have a volume of 487.52 Å^3 in compound **3a** and 471.76 Å^3 in compound **3b**, which account for 28% and 27% of their unit cell size, respectively. They are formed along the *a* crystallographic axis (Figure 3).
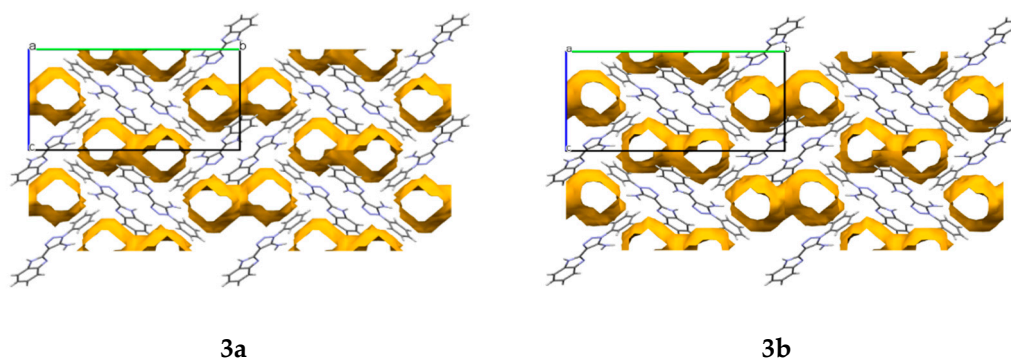

3a **3b**

Figure 3. The cavities with solvent molecules formed in crystals **3a** and **3b**.

Modern crystal engineering is based on various approaches to the crystal structure analysis, including the close packing principles of Kitaigorodskii [27], the Popelier's principles [28], the set of graphs applied to the crystal structure analysis [29], the Etter's rules [30], or the Desiraju's concept of supramolecular synthons [31–33]. All these approaches are based mainly on the study and geometric parameters comparison of intermolecular interactions. The modern basic method is the concept of supramolecular synthons, which allows us to describe a crystal as a packing of molecular assemblies bound by any specific intermolecular interactions (hydrogen or halogen bonds, stacking interaction, etc. [31–33]). This concept turned out to be very useful and has made significant progress in studying and predicting the crystal structure [32]. Nevertheless, the release of the basic supramolecular synthon is reliable in the presence of only one strong intermolecular interaction. This task becomes very equivocal in the presence of two or more strong hydrogen bonds, or weak interactions with close geometric parameters, or when specific intermolecular interactions are absent at all. For example, as shown earlier, the application of the geometric approach has proved to be unsuccessful in determining the strongest intermolecular interaction in crystals of diaminobenzenes and nitro-diaminobenzenes [34,35].

The analysis of interatomic distances in crystal **3** indicates the presence of a set of intermolecular C–H . . . X H-bonds, one N-H . . . N hydrogen bond and stacking interaction with a "head-to-head" orientation (Table 2). Based on their geometrical parameters, it is possible to suggest that all of these interactions are weak, except for N2-H2N . . . N3' H-bond (Table 2). In crystals **3a** and **3b**, the number of C-H...X interactions is reduced (Table 3). In these crystals, the set of intermolecular interactions is almost identical. It should be noted that the N2-H2N . . . N3' hydrogen bond and the hydrogen bond formed between the amino group and the solvate molecule are also stronger than others (Table 3). Visual analysis of crystal structures **3**, **3a** and **3b** allows us to recognize the centrosymmetric dimers bound by the N2-H2N . . . N3' and C5-H5 . . . N4' hydrogen bonds (Figure 4, Tables 2 and 3). These dimers are packed in the layers due to the stacking interactions (Figure 5). Ergo, routine analysis of specific intermolecular interactions in the crystal does not allow us to make definite conclusions about the preferred packing arrangement of molecules and the role of weak hydrogen bonds. This may be done only on the basis of consideration of topology of interactions between molecules in terms of their directionality and energies.

Table 2. Intermolecular interactions in **3** crystal.

Interaction	Operation of Symmetry	H ... A, Å	D-H ... A, Degree
N2-H2N ... N3	1 − x, 2 − y, 1 − z	2.14	165
C5-H5 ... N4	1 − x, 2 − y, 1 − z	2.69	139
C2-H2 ... C14	0.5 − x, 0.5 + y, 0.5 − z	2.89	140
C3-H3 ... C12	0.5 + x, 1.5 − y, −0.5 + z	2.85	141
C14-H14 ... C2	0.5 − x, 1.5 + y, 0.5 − z	2.88	138
C15-H15 ... N1	0.5 − x, 0.5 + y, 0.5 − z	2.73	129
N4 ... C11	0.5 − x, 1.5 + y, 0.5 − z	3.12	

Table 3. Intermolecular interactions in **3a** and **3b** crystals.

Interaction	Operation of Symmetry	3a		3b	
		H ... A, Å	D-H ... A, deg.	H ... A, Å	D-H ... A, deg.
N2-H2N ... N3	2 − x, 1 − y, 1 − z	2.14	163	2.12	162
C5-H5 ... N4	2 − x, 1 − y, 1 − z	2.70	139	2.70	138
C14-H14 ... C9	0.5 − x, 1.5 + y, 0.5 − z	2.87	138	2.74	145
C9 ... C5	1 − x, 1 − y, 1 − z	3.38		3.43	
N6-H6NA ... O1S	x, y, z	2.15	153		
N6-H6NA ... N1S	x, y, z			2.08	171

3　　　　　　　　　**3a**　　　　　　　　　**3b**
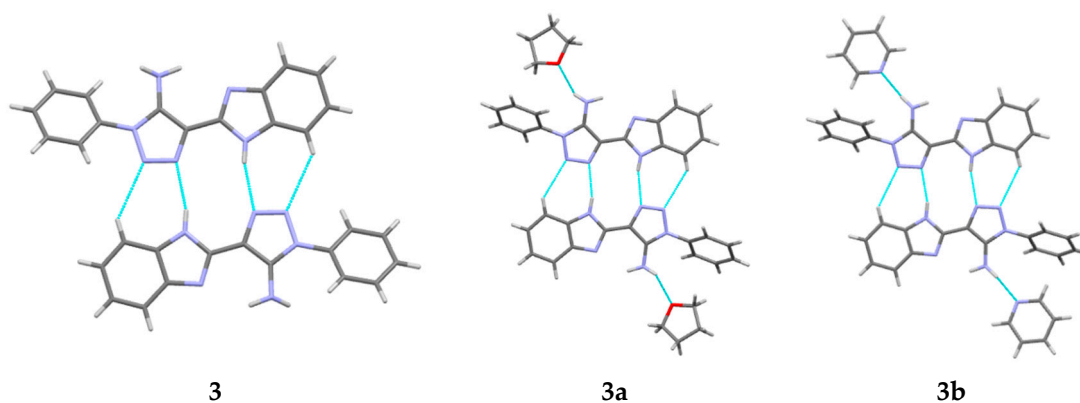
Figure 4. Centrosymmetric dimers in crystals **3**, **3a** and **3b**.

3

Figure 5. *Cont.*
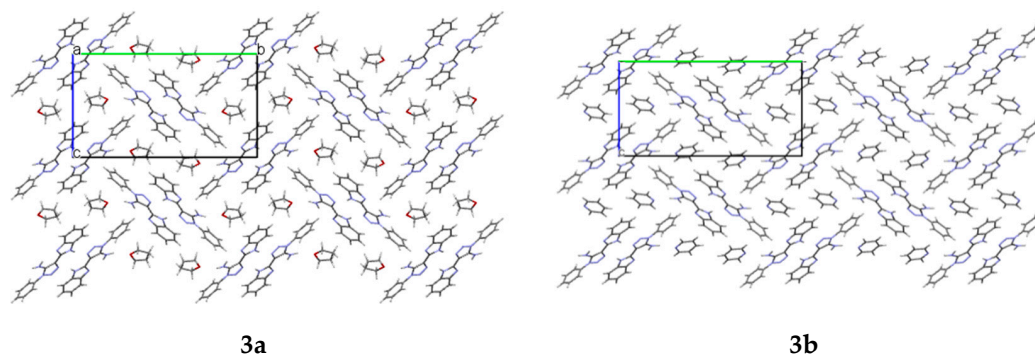
3a　　　　　　　　　　　　　　　**3b**
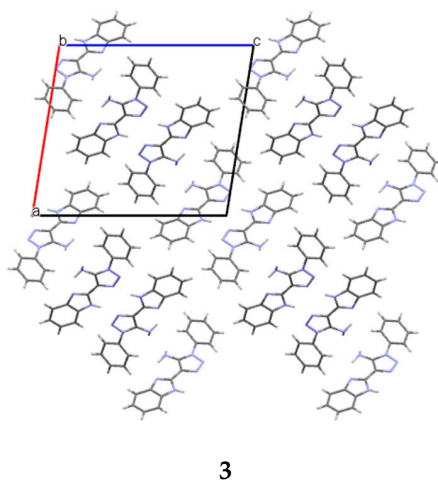
Figure 5. Packing of molecules in crystals **3**, **3a** and **3b**. The projections along the [0 1 0] (on top) and [1 0 0] (on bottom) crystallographic directions are presented.

In terms of the energy of interactions between molecules, the study of the crystal structure was carried out using the method described previously [36,37] (calculation procedure is presented in detail in the Materials and Methods Section). This method does not depend on the nature of specific intermolecular interactions and their geometric parameters and takes into account all possible types of the intermolecular interactions. The first coordination sphere for each of the molecules located in the asymmetric part of the unit cell contains 16–27 molecules in the crystals of compounds **3**, **3a** and **3b**. Data for dimers with interaction energies higher than 1% of the total interaction energy of the basic molecule with all the molecules belonging to its first coordination sphere are given in Tables 4–6.

Table 4. Symmetry codes, bonding type, interaction energy of the basic molecule with neighboring ones (E_{int}, kcal/mol) with the highest values (more than 1 % of the total interaction energy) and the contribution of this energy to the total interaction energy (%) in crystals of **3**.

Dimer	Symmetry Operation	E_{int}, kcal/mol	Contribution to the Total Interaction Energy, %	Interaction Type
3-d1	x, 1 + y, z	−14.04	16.5	Stacking 3.48 Å
3-d2	x, −1 + y, z	−14.04	16.5	Stacking 3.48 Å
3-d3	1/2 − x, 1/2 + y, 1/2 − z	−6.07	7.1	C-H . . . π 2.78 Å, N-H . . . N 2.73 Å
3-d4	1/2 − x, 3/2 + y, 1/2 − z	−3.21	3.8	C-H . . . π 2.77 Å
3-d5	1/2 − x, −1/2 + y, 1/2 − z	−6.07	7.1	C-H . . . π 2.78 Å, N-H . . . N 2.73 Å
3-d6	1/2 − x, −3/2 + y, 1/2 − z	−3.21	3.8	C-H . . . π 2.77 Å
3-d7	3/2 − x, 1/2 + y, 1/2 − z	−1.98	2.3	C-H . . . π 2.80 Å
3-d8	3/2 − x, −1/2 + y, 1/2 − z	−1.98	2.3	C-H . . . π 2.80 Å
3-d9	−x, −y, 1 − z	−1.43	1.7	Non-specific
3-d11	1 − x, 1 − y, 1 − z	−7.56	8.9	C-H . . . π 2.80 Å
3-d12	1 − x, 2 − y, 1 − z	−17.90	21.0	N-H . . . N 1.99 Å, C-H . . . N 2.58 Å
3-d13	1/2 + x, 1/2 − y, −1/2 + z	−1.98	2.3	C-H . . . π 2.99 Å
3-d14	1/2 + x, 3/2 − y, −1/2 + z	−1.84	2.2	C-H . . . π 2.72 Å
3-d15	−1/2 + x, 1/2 − y, 1/2 + z	−1.98	2.3	C-H . . . π 2.99 Å
3-d16	−1/2 + x, 3/2 − y, 1/2 + z	−1.84	2.2	C-H . . . π 2.72 Å

The analysis of pairwise interaction energies in the crystal of **3** has revealed that the first coordination sphere of the basic molecule contains 16 neighboring molecules. The calculations of the pairwise interaction energies of the basic molecule with each of its neighbors have revealed one strong interaction and two weaker interactions (Table 4). The strongest bonded dimer 3-d12 (Figure 6) is formed due to classic N-H . . . N and C-H . . . N hydrogen bonds, while the molecules within two other strongly bonded dimers 3-d1 and 3-d2 are linked by the stacking interaction with the "head to head"

orientation (Table 4). As a result, the double column (Figure 7) can be recognized as the primary basic structural motif (BSM1) in the crystal of **3**. The interaction energy of each molecule with its neighbors within the column is −53.54 kcal/mol. The molecules belonging to the neighboring columns are bound by the C-H . . . π and N-H . . . N hydrogen bonds. The interaction energies of the primary BSM with neighboring columns are anisotropic enough. It allows to separate out the layer parallel to the (−1 0 1) crystallographic plane as the second basic structural motif (BSM2) (Figure 7) where the interaction energy between neighboring layers is almost ten times smaller than the interaction energy within the layer (−72.10 kcal/mol). The neighboring layers are bound by the C-H . . . π hydrogen bonds and non-specific interactions. Therefore, we can conclude that crystal **3** has two levels of organization and can be classified as columnar-layered.
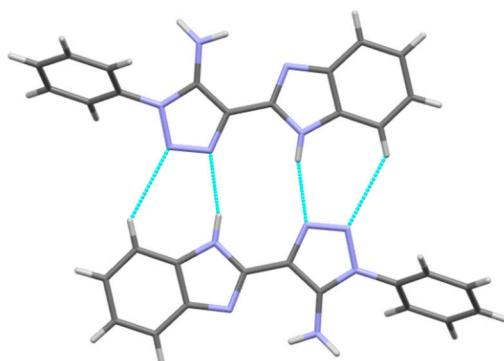

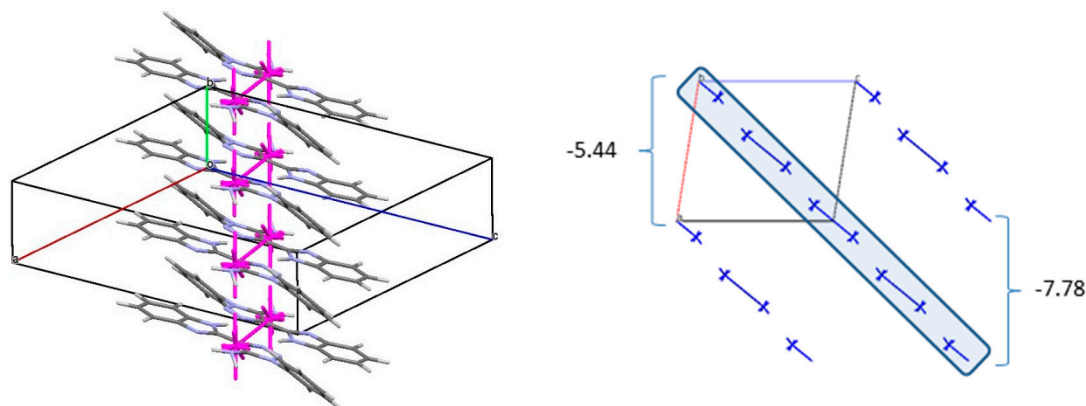**Figure 6.** The dimer with the highest interaction energy in the crystals of **3**, **3a** and **3b**.

Figure 7. View of the double column as the primary BSM (**Left**) and packing of the layers; the projection along the *b* crystallographic direction (**Right**) in terms of the energy-vector diagrams in the crystal of **3**.

The introduction of the solvent molecule into the crystal causes some change in the crystal organization. The analysis of pairwise interaction energies has revealed that the first coordination sphere of the basic molecule **3** contains 16 neighboring molecules in both solvates while the solvate molecule is surrounded by 11 neighboring molecules in crystal **3a** and 9 neighboring molecules in crystal **3b** (Tables 5 and 6). Similar to crystal **3**, the most strongly bound dimer 3a-d8 and 3b-d8 is formed due to classic N-H . . . N and C-H . . . N hydrogen bonds, while the molecules within another strongly bound dimer 3a-d7 and 3b-d7 are linked by the stacking interaction with "head to tail" orientation (Tables 5 and 6). As a result, the zig-zag columns can be recognized as the primary basic structural motif (BSM1) in crystals **3a** and **3b** (Figure 8). The molecules within the columns are also bound by two strongest interactions, and the interaction energies of the basic molecule with its neighbors within the column are −42.15 kcal/mol (**3a**) and −40.30 kcal/mol (**3b**). The molecules belonging to the neighboring columns are bound by the N-H . . . O1S in **3a**, N-H . . . N1S in **3b**, C-H . . . π and C-H . . . N hydrogen bonds and non-specific interactions. The interactions of the primary BSM

with neighboring columns are almost isotropic because of the interaction energies vary in the range of −4.24 ÷ −9.22 kcal/mol (**3a**) and −6.10 ÷ −9.33 kcal/mol (**3b**) (Figure 8). The interaction energy between the neighboring columns is several times smaller than the interaction energy within the column. Thus we can conclude that the crystals **3a** and **3b** have only one level of organization and can be classified as columnar. It should be noted that despite different solvent molecules in crystals **3a** and **3b**, their crystal packings are almost isostructural (Figure 8).

Table 5. Symmetry codes, bonding type, and interaction energy of the basic molecule with neighboring ones (E_{int}, kcal/mol) with the highest values (more than 1% of the total interaction energy) and the contribution of this energy to the total interaction energy (%) in crystal **3a**.

Dimer	Symmetry Operation	Molecule–Solvate or Molecule–Molecule Interaction	E_{int}, kcal/mol	Contribution to the Total Interaction Energy, %	Interaction Type
3a-d1	x, y, z	M-S	−6.32	7.5	N-H … O1S 2.01 Å
3a-d2	1 + x, y, z	M-M	−5.50	6.5	C-H … N 2.72 Å
3a-d3	1 + x, y, z	M-S	−2.52	3.0	Non-specific
3a-d4	−1 + x, y, z	M-M	−5.50	6.5	C-H … N 2.72 Å
3a-d5	−x, −1/2 + y, 1/2 − z	M-S	−1.30	1.5	Non-specific
3a-d6	1 − x, −1/2 + y, 1/2 − z	M-S	−2.38	2.8	Non-specific
3a-d7	1 − x, 1 − y, 1 − z	M-M	−12.98	15.4	Stacking 3.40 Å
3a-d8	2 − x, 1 − y, 1 − z	M-M	−18.17	21.5	N-H … N 1.99 Å, C-H … N 2.58 Å
3a-d9	x, 3/2 − y, 1/2 + z	M-M	−4.81	5.7	C-H … π 2.84 Å, C-H … N 2.67 Å
3a-d10	x, 3/2 − y, 1/2 + z	M-S	−2.29	2.7	Non-specific
3a-d11	x, 3/2 − y, −1/2 + z	M-M	−4.81	5.7	C-H … π 2.84 Å, C-H … N 2.67 Å
3a-d12	x, 3/2 − y, −1/2 + z	M-S	−4.24	5.0	C-H … π 2.83 Å
3a-d13	1 + x, 3/2 − y, 1/2 + z	M-S	−3.17	3.8	C-H … π 2.95 Å
3a-d14	1 + x, 3/2 − y, 1/2 + z	M-M	−4.41	5.2	C-H … N 2.65 Å
3a-d15	−1 + x, 3/2 − y, −1/2 + z	M-M	−4.41	5.2	C-H … N 2.65 Å
3a-d16	−1 + x, 3/2 − y, −1/2 + z	M-S	−1.75	2.1	Non-specific
3a-d17	x, y, z	S-M	−6.32	23.6	N-H … O1S 2.01 Å
3a-d19	−1 + x, y, z	S-M	−2.52	9.4	Non-specific
3a-d21	−x, 1/2 + y, 1/2 − z	S-M	−1.30	4.9	Non-specific
3a-d22	1 − x, 1/2 + y, 1/2 − z	S-M	−2.38	8.9	Non-specific
3a-d23	1 − x, 2 − y, 1 − z	S-S	−1.17	4.4	Non-specific
3a-d24	x, 3/2 − y, 1/2 + z	S-M	−4.24	15.8	C-H … π 2.83 Å
3a-d25	x, 3/2 − y, −1/2 + z	S-M	−2.29	8.6	Non-specific
3a-d26	1 + x, 3/2 − y, 1/2 + z	S–M	−1.75	6.5	Non-specific
3a-d27	−1 + x, 3/2 − y, −1/2 + z	S-M	−3.17	11.9	C-H … π 2.95 Å

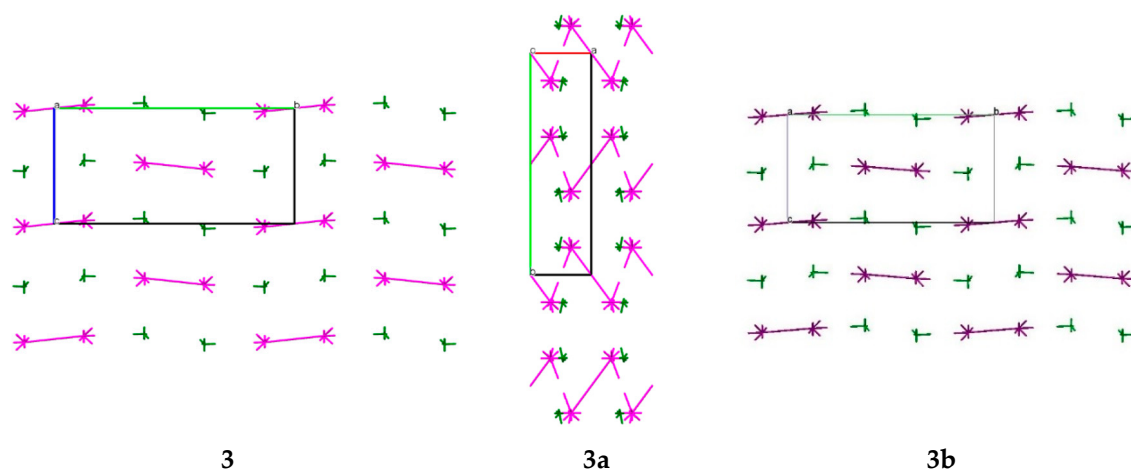**3**　　　　　　　　　　**3a**　　　　　　　　　　**3b**

Figure 8. View of the double column as the primary BSM (middle) and packing of the columns (left and right), the projection along *a* (left, right) and *c* (middle) crystallographic directions in terms of the energy-vector diagrams in crystals **3a** and **3b**.

Table 6. Symmetry codes, bonding type, and interaction energy of the basic molecule with neighboring ones (E_{int}, kcal/mol) with the highest values (more than 1% of the total interaction energy) and the contribution of this energy to the total interaction energy (%) in crystal **3b**.

Dimer	Symmetry Operation	Type of Interaction	E_{int}, kcal/mol	Contribution to the Total Interaction Energy, %	Interaction Type
3b-d1	x, y, z	M-S	−9.33	10.7	N-H … N1S 2.01 Å
3b-d2	1 + x, y, z	M-M	−4.91	5.6	C-H … N 2.65 Å
3b-d3	1 + x, y, z	M-S	−2.76	3.2	Non-specific
3b-d4	−1 + x, y, z	M-M	−4.91	5.6	C-H … N 2.65 Å
3b-d5	−x, −1/2 + y, 1/2 − z	M-S	−1.15	1.3	Non-specific
3b-d6	1 − x, −1/2 + y, $\frac{1}{2}$ − z	M-S	−2.61	3.0	Non-specific
3b-d7	1 − x, 1 − y, 1 − z	M-M	−13.00	15.0	Stacking 3.40 Å
3b-d8	2 − x, 1 − y, 1 − z	M-M	−17.48	20.1	N-H … N 1.98 Å, C-H … N 2.58 Å
3b-d9	x, 3/2 − y, 1/2 + z	M-M	−2.75	3.2	Non-specific
3b-d10	x, 3/2 − y, 1/2 + z	M-S	−4.81	5.5	C-H … π 2.88 Å, C-H … N 2.62 Å
3b-d11	x, 3/2 − y, −1/2 + z	M-M	−4.79	5.5	C-H … π 2.88 Å
3b-d12	x, 3/2 − y, −1/2 + z	M-S	−4.81	5.5	C-H … π 2.88 Å, C-H … N 2.62 Å
3b-d13	1 + x, 3/2 − y, 1/2 + z	M-S	−3.35	3.9	C-H … π 2.80 Å
3b-d14	1 + x, 3/2 − y, $\frac{1}{2}$ + z	M-M	−4.50	5.2	H … H 2.34 Å
3b-d15	−1 + x, 3/2 − y, −1/2 + z	M-M	−4.50	5.2	H … H 2.34 Å
3b-d16	−1 + x, 3/2 − y, −1/2 + z	M-S	−1.26	1.5	H … H 2.28 Å
3b-d17	x, y, z	S-M	−9.33	31.8	N-H … N1S 2.01 Å
3b-d18	−1 + x, y, z	S-S	−2.76	9.4	Non-specific
3b-d19	−x, 1/2 + y, 1/2 − z	S-M	−1.15	3.9	Non-specific
3b-d20	1 − x, 1/2 + y, $\frac{1}{2}$ − z	S-S	−2.61	8.9	Non-specific
3b-d21	1 − x, 2 − y, 1 − z	S-M	−1.38	4.7	Non-specific
3b-d22	x, 3/2 − y, 1/2 + z	S-M	−4.79	16.3	C-H … π 2.88 Å
3b-d23	x, 3/2 − y, −1/2 + z	S-S	−2.75	9.4	Non-specific
3b-d24	1 + x, 3/2 − y, 1/2 + z	S-M	−1.26	4.3	H … H 2.28 Å
3b-d25	−1 + x, 3/2 − y, −1/2 + z	S-M	−3.35	11.4	C-H … π 2.80 Å

The comparison of the results of the crystal structure analysis performed by two ways shows clearly that the geometrical characteristics of intermolecular interactions are not informative enough to separate out the main structural motif and study the comparative role of different types of interactions. At the same time, the study of interaction energies between molecules allows us to recognize different levels of crystal structure organization and describe the interaction types causing their formation. Thus, the classic N-H … N and C-H … N hydrogen bonds play the main role in all the studied crystals forming the primary basic structural motif. Their role is comparable with the role of the stacking interactions. The inclusion of the solvent molecules in the crystals **3a** and **3b** lead to a more isotropic packing type.

2.3. Molecular Docking Simulations

The title molecule was tested as a potential agent capable of interacting with capsid of hepatitis B virus (HBV) and thus inhibit its replication [38–40]. The title molecule has been tested as a potential analogue of ligands of protein complexes 5E0I, 5T2P, 5WRE, and 5GMZ. The X-ray crystallographic structures of such ligand-protein complexes are known from [40].

The pharmacophore model and docking procedure were performed by using computer the program complex Ligandscout 4.3 [41]. All the above-mentioned protein structures contain six chains (A, B, C, D, E, and F). According to our preliminary calculations, the residual mean square deviations (RMSD) between docking-generated poses for reference molecule and poses obtained from x-ray data were minimal (RMSD < 1 Å) for D-chains. Therefore, D-site was selected for in silico modeling as the site of the ligand-protein interactions. The LigandScout option was used for pharmacophore generation, and then the title molecule was docked at D-site. The obtained data for score functions

are presented in Table 7 (for the description of estimated parameters, see the LigandScout manual). One can see that the title molecule has significant interactions with the corresponding proteins.

Table 7. Parameters of ligand-protein interactions of the title molecule (binding site is D chain for all proteins).

Protein	Binding Affinity Score	Est. Binding Energy (kcal/mol)
5E0I	−15.8	−14.06
5GMZ	−16.5	−14.6
5WRE	−14.0	−14.0
5T2P	−20.7	−15.5

To illustrate, two receptor-ligand complexes (with 5GMZ and 5T2P) are shown in Figure 9.
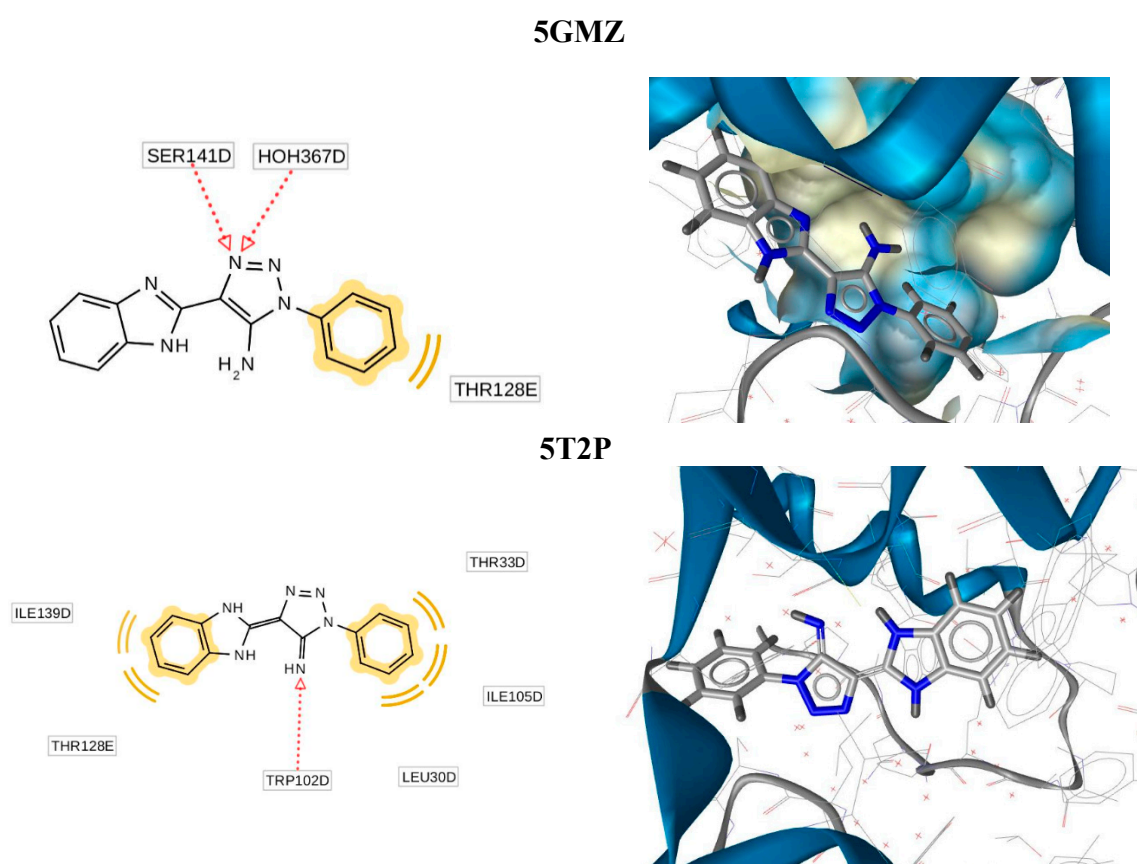
5GMZ

5T2P

Figure 9. Generated docking poses for complexes of compound **3** with 5GMZ and 5T2P proteins.

In the 2D pictures in Figure 8, the hydrogen bond acceptor is designated by the red dotted line, and the hydrophobic interaction is designated by the curved yellow line. It should also be noted that in the two presented examples, different tautomeric forms of the studied molecule generated by docking procedure form stable ligand-protein complexes.

2.4. Anti-Hepatitis B Virus (HBV) Activity

The biological activity of compound **3** was studied using an experimental in vitro hepatitis B virus infection model based on human hepatoma line HepG2 stably transfected with the NTCP gene [42]. This model, which maintains a full virus replication cycle, was developed in our laboratories for identification of viral entry inhibitors, promising candidates to prevent development of resistant HBV forms [43]. The title molecule **3** demonstrated 86% inhibition of HBV replication (in 10 μM

concentration) in this model. Taking into account the recently reported test results for viral entry inhibition of FDA approved drugs zafirlukast (IC_{50} 6.5 µM), TRIAC (IC_{50} 6.9 µM), and sulfasalazine (IC_{50} 9.6 µM) [44], compound **3** can be considered as a promising starting point for the development of potent viral entry inhibitors capable to prevent development of resistant HBV forms.

3. Materials and Methods

3.1. Chemistry

3.1.1. General Information

All chemicals were obtained from Sigma-Aldrich or Merck. All NMR spectra were recorded on a Varian MR-400 spectrometer (Varian, Inc., Walnut Creek, CA, USA) with standard pulse sequences operating at 400 MHz for 1H NMR and 100 MHz for 13C NMR. For NMR spectra, DMSO-d6 was used as solvent. Liquid chromatography mass spectrometry was developed by means of chromatography with PHENOMENEX GEMINI NX C18 110 Å 4.61 × 150 mm column (0.05% TFA, gradient ACN/H2O), UV-detector SHIMADZU SPD-10AD VP (registered absorption at 254 nm), ELSD (evaporative light scattering detector) SEDEX-75 (S.E.D.E.R.E., PARC VOLTA-BP 27 9, Rue Parmentier 94141 Alfortville Cedex FRANCE) and API-150EX mass-spectrometer (MDS Sciex, Toronto, ON, Canada). Elution started with 0.1 M solution of TFA in water and ended with 0.1 M solution of TFA in acetonitrile used a linear gradient at a flow rate of 0.15 mL/min and an analysis cycle time of 25 min. The FT-IR spectrum was registered in a KBr pellet with a Shimadzu IR Prestige-21 Fourier Transform Infrared (FTIR) Spectrophotometer (Shimadzu Corporation, Kyoto, Japan). The UV/Vis spectrum was registered in acetonitrile with an Agilent 8453 UV-visible Spectrophotometer. The melting point was registered with a Buchi M-560 (Buchi AG, Meierseggstrasse 40, 9230 Flawil, Switzerland). Elemental analysis was performed on EuroEA-3000 CHNS-O Analyzer (Euro Vector, Via Tortona 5-20144, Milan, Italy).

3.1.2. Synthesis and Crystallization of Compound **3**

Azidobenzene **1** (1.1 mmol, 131 mg) and 2-(1*H*-benzo[d]imidazol-2-yl)acetonitrile 2 (1.0 mmol, 157 mg) were added with vigorous stirring to the solution of sodium methoxide prepared from sodium (5.0 mmol, 115 mg) and methanol (20 mL). The mixture was stirred and heated for 2 h at 70 °C and then cooled down to a room temperature. The solution was diluted with water (50 ml). The formed precipitate was collected by filtration, washed with water and *i*-PrOH, recrystallized from acetonitrile (10 mL), filtered off, washed with acetonitrile (2 mL) and dried to give pure product **3**. Yield 260 mg (94%), white powder, m.p. 205–206 °C; UV (Acetonitrile) λ_{max} (ε): 231 nm (shoulder) (26300), 264 nm (12400), 274 nm (12800), 301 nm (34200), 312 nm (30900) (Figure S1); IR (KBr): ν (cm^{-1}) 3390 (N–H), 3260 (N–H), 3177 (N–H), 3067 (C–H), 1626 (C=N), 1591, 1554, 1502, 1453, 1422, 1341, 1284, 1270, 1145, 1101, 1047, 993, 958, 927, 764, 743, 696, 653, 626, 595, 482 (Figure S2); ^{13}C NMR (100 MHz, DMSO-d$_6$): δ 146.50, 143.34, 142.49, 135.06, 133.78, 129.78 (2C), 129.01, 123.85 (2C), 121.80, 121.48, 119.99, 117.90, 111.06; (Figure S3); ^{1}H NMR (400 MHz, DMSO-d6): δ 12.97 (s, 1H, NH), 7.74 – 7.54 (m, 6H), 7.47 (s, 1H), 7.17 (dd, J = 6.2, 2.9 Hz, 2H), 6.71 (s, 2H, NH$_2$); (Figure S4); LC/MS m/z (%): 277.0 [MH]$^+$ (100); 249.0 [MH-N2]$^+$ (100); (Figure S5); Found, %: C 65.03; H 4.40; N 30.47. $C_{15}H_{12}N_6$. Calculated, %: 65.21; H 4.38; N 30.42.

Further crystallization by slow evaporation of a solution of **3** in acetonitrile was carried out to provide single stick-like colorless crystals suitable for X-ray diffraction analysis. Compounds **3a** and **3b** were obtained by recrystallization of **3** from THF and pyridine, respectively.

3.2. X-Ray Diffraction Study

The crystals of **3** ($C_{15}H_{12}N_6$) are monoclinic. At 293 K a = 15.673(3) Å, b = 4.7447(8) Å, c = 17.615(3) Å, β = 99.067(17), V = 1293.6(4) Å^3, M_r =276.31, Z = 4, space group $P2_1/n$, d$_{calc}$= 1.419 g/cm^3, m(MoK$_a$) = 0.092 mm^{-1}, F(000) = 576. Intensities of 9060 reflections (2282 independent, R$_{int}$ = 0.102) were

measured on the «Xcalibur-3» diffractometer (graphite monochromated MoKα radiation, CCD detector, ω-scaning, 2Θmax = 50°).

The crystals of **3a** ($C_{19}H_{20}N_6O$) are monoclinic. At 293 K a = 6.2541(6) Å, b = 22.4997(15) Å, c = 12.8291(14) Å, β = 100.521(10)°, V = 1774.9(3) Å^3, M_r =348.41, Z = 4, space group P2$_1$/c, d_{calc}= 1.304 g/cm^3, m(MoK$_a$) = 0.086 mm^{-1}, F(000) = 736. Intensities of 11257 reflections (3131 independent, R$_{int}$ = 0.092) were measured on the «Xcalibur-3» diffractometer (graphite monochromated MoKα radiation, CCD detector, ω-scaning, 2Θmax = 50°).

The crystals of **3b** ($C_{20}H_{17}N_7$) are monoclinic. At 293 K a = 6.4192(13) Å, b = 23.082(5) Å, c = 12.161(3) Å, β = 99.75(2)°, V = 1775.8(7) Å^3, M_r =355.4, Z = 4, space group P2$_1$/c, d_{calc}= 1.329 g/cm^3, m(MoK$_a$) = 0.085 mm^{-1}, F(000) = 744. Intensities of 12081 reflections (3135 independent, R$_{int}$ = 0.125) were measured on the «Xcalibur-3» diffractometer (graphite monochromated MoKα radiation, CCD detector, ω-scaning, 2Θmax = 50°).

The structures were solved by direct method using SHELXTL package [45]. Position of the hydrogen atoms were located from electron density difference maps and refined by "riding" model with U_{iso} = nU_{eq} of the carrier atom (n = 1.2 for all hydrogen atoms). Full-matrix least-squares refinement of the structures against F^2 in anisotropic approximation for non-hydrogen atoms using 2282 (**3**), 3131 (**3a**), reflections was converged to: wR_2 = 0.156 (R_1 = 0.059 for 1192 reflections with F > 4σ(F), S = 0.928) for structure **3**, wR_2 = 0.188 (R_1 = 0.072 for 1736 reflections with F>4σ(F), S = 0.973) for structure **3a**, wR_2 = 0.183 (R_1 = 0.075 for 1537 reflections with F > 4σ(F), S = 0.923) for structure **3b**. The final atomic coordinates, and crystallographic data for molecules **3**, **3a**, **3b** have been deposited to with the Cambridge Crystallographic Data Centre, 12 Union Road, CB2 1EZ, UK (fax: +44-1223-336033; e-mail: deposit@ccdc.cam.ac.uk) and are available on request quoting the deposition number CCDC 1958899 for **3**, 1958898 for **3a**, 1958900 for **3b**).

3.3. Theoretical Calculations

Analysis of the **3**, **3a** and **3b** crystal structures was performed using an approach based on the calculations of the energies of pair interactions between molecules in a crystal [36,37]. The first coordination sphere of the basic M0 molecule was constructed using the standard procedure in Mercury program (version 4.0, Cambridge, UK) [46]. This procedure was applied individually to each molecule found in the asymmetric part of the unit cell. The observed cluster was taken from X-ray diffraction data and was divided on the dimers in which one molecule M0 is the basic molecule and the second molecule Mi is one of the molecules of its first coordination sphere. The positions of the hydrogen atoms were normalized to 1.089 Å for C-H and 1.015 Å for N-H bonds taking into account the geometry optimization results of isolated molecules. The need for such a procedure is due to the fact that the X-H bonds determined by the X-ray structural study are reduced due to the peculiarities of the method [47]. The energies of pairwise interactions were calculated using the density functional method B97-D3 with Def2-TZVP basis set (B97-D3/ Def2-TZVP) and were adjusted for the BSSE correction [48]. The B97-D3 functional has been evaluated as one of the most reliable dispersion-corrected functional for the calculation of intermolecular interactions [49,50]. The calculations were performed using ORCA software (Max Plank Institute for Chemical Energy Conversion, Version 3.0.3, Ruhr, Germany) [51].

The analysis of the obtained data is based on the assumption that the values of the interaction energies can take on vector properties, since them originate in the geometric center of the basic molecule, and each of them is directed to the geometric center of one of the adjacent molecules [35]. Each length of such an energy vector is normalized to the strongest energy of pairwise interaction by the equation:

$$L_i = (R_i E_i)/2E_{str}, \tag{1}$$

where R_i is the distance between the geometric centers of the interacting molecules, E_i is the interaction energy between the two molecules, and E_{str} is the energy of the strongest pair interaction in the crystal.

The purpose of such normalization is to make the length of the vector almost independent of the method of calculation. Replacing a molecule with its vector image and applying symmetry operations make it possible to construct an energy vector diagram (EVD) of a molecule and to study the energy structure instead of the large number of intermolecular interactions.

3.4. Docking Studies

The pharmacophore model generation and docking were performed using Ligandscout 4.3 program [41].

4. Conclusions

A new representative of "benzimidazole–1,2,3-triazole" dual moiety molecules, 4-(1*H*-benzo[d]imidazol-2-yl)-1-phenyl-1*H*-1,2,3-triazol-5-amine (**3**), and its solvates with THF (**3a**) and pyridine (**3b**) have been synthesized and studied using both theoretical and experimental methods. The studied compounds were characterized by spectral methods, and their molecular and crystal structures were confirmed by X-ray diffraction study. Quantum-chemical calculations were used to study the energies of interactions between molecules to recognize different levels of crystal structure organization and describe the interaction types causing their formation. Analysis of topology of intermolecular interactions in terms of their energy and directionality indicated columnar-layered structure of the crystal **3**. The inclusion of the solvent molecules in the crystals **3a** and **3b** led to more isotropic packing type which could be classified as columnar. The ligand-receptor interactions between compound **3** and its potential hepatitis B viral targets were modeled using the molecular docking approach. At the final stage of this work, experimental in vitro biological studies confirmed that compound **3** is a potent HBV replication inhibitor with IC_{50} in a low micromolar range. The comparative literature data demonstrated that the described chemotype could be considered as a promising starting point for the development of anti-HBV drugs capable of preventing development of resistant viral forms.

Supplementary Materials: The following are available online at http://www.mdpi.com/2073-4352/9/12/644/s1, Figure S1: UV/Vis spectrum of the title compound 3 (acetonitrile); Figure S2. IR spectrum of the title compound 3 (KBr pellet); Figure S3. ^{13}C NMR (100 MHz, DMSO-d6) spectrum of the title compound 3; Figure S4. ^{1}H NMR (400 MHz, DMSO-d6) spectrum of the title compound 3; Figure S5. LC/MS Data for Structural Determination of of the title compound 3

Author Contributions: A.V.I., O.D.M.: Conceived and designed the experiments; Analyzed and interpreted the data; Contributed reagents, materials, analysis tools or data; Wrote the paper; Final approval of the version submitted. D.V.K., S.M.K.: Conceived and designed the experiments; Analyzed and interpreted the data; critically revising its important intellectual content. S.V.S., I.S.K.: Performed the X-ray experiments; Analyzed and interpreted the data. N.D.B., I.G.D.: Analyzed and interpreted the data; Contributed reagents, materials, analysis tools or data; Wrote the paper. V.V.I., O.D.K. and T.L.: Performed quatum-chemical calculations; Analyzed and interpreted the data; Contributed reagents, materials, analysis tools or data.

Conflicts of Interest: The authors declare no conflict of interest.

References

1. Bräse, S. *Privileged Scaffolds in Medicinal Chemistry. Design, Synthesis, Evaluation*; RSC: Cambridge, UK, 2015.
2. Verma, A.; Ram Yadav, M.; Giridhar, R.; Prajapati, N.; Tripathi, A.C.; Saraf, S.K. Nitrogen containing privileged structures and their solid phase combinatorial synthesis. *Comb. Chem. High Throughput Screen.* **2013**, *16*, 345–393. [CrossRef]
3. Welsch, M.E.; Snyder, S.A.; Stockwell, B.R. Privileged scaffolds for library design and drug discovery. *Curr. Opin. Chem. Biol.* **2010**, *14*, 347–361. [CrossRef] [PubMed]

4. Marinescu, M. *Chemistry and Applications of Benzimidazole and Its Derivatives*; IntechOpen: London, UK, 2019. [CrossRef]

5. Neelima, S.; Naim, M.J.; Alam, J.; Nawaz, F.; Shujauddin, A.; Alam, O. Benzimidazole Scaffold as Anticancer Agent: Synthetic Approaches and Structure–Activity Relationship. *Arch. Pharm. Chem. Life Sci.* **2017**, *350*, 1–80.

6. Mann, J.; Baron, A.; Opoku Boahen, Y.; Johansoon, E.; Parkmson, G.; Kelland, L.R.; Neidle, S. A new class of symmetric bisbenzimidazole-based DNA minor groove-binding agents showing antitumor activity. *J Med. Chem.* **2001**, *44*, 138–142. [CrossRef] [PubMed]

7. Achar, K.C.; Hosamani, K.M.; Seetharamareddy, H.R. In-vivo analgesic and anti-inflammatory activities of newly synthesized benzimidazole derivatives. *Eur. J. Med. Chem.* **2010**, *45*, 2048–2054. [CrossRef] [PubMed]

8. Ramya, V.S.; Kallappa, M.H.; Rangappa, S.K.; Mallinath, H.H. Derivatives of benzimidazole pharmacophore: Synthesis, anticonvulsant, antidiabetic and DNA cleavage studies. *Eur. J. Med. Chem.* **2010**, *45*, 1753–1759.

9. Patricia, T.; Hugo, A.K.; Bruno, P.; Fernando, L.; Aurélie, P.; Christophe, B.; Rodrigo, A. Organometallic benzimidazoles: Synthesis, characterization and antimalarial activity. *Inorganic Chem. Commun.* **2013**, *35*, 126–129.

10. Ozden, S.; Atabey, D.; Yildiz, S.; Goker, H. Synthesis and potent antimicrobial activity of some novel methyl or ethyl 1H-benzimidazole-5-carboxylates derivatives carrying amide or amidine groups. *Bioorg Med. Chem.* **2005**, *13*, 1587–1590. [CrossRef]

11. Goker, H.; Ku, C.; Boykin, D.W.; Yildiz, S.; Altanlar, N. Synthesis of some new 2-substituted-phenyl-1H-benzimidazole-5-carbonitriles and their potent activity against Candida species. *Bioorg Med. Chem.* **2002**, *10*, 2589–2594. [CrossRef]

12. Buckle, D.R.; Rockell, C.J.M.; Smith, H.; Spicer, B.A. Studies on 1,2,3-triazoles. 13. (Piperazinylalkoxy)-[1]benzopyrano[2,3-d]-1,2,3-triazol-9(1H)-ones with combined H1-antihistamine and mast cell stabilizing properties. *J. Med. Chem.* **1986**, *29*, 2262–2267. [CrossRef]

13. Alvarez, R.; Velazquez, S.; San-Felix, A.; Aquaro, S.; De Clercq, E.; Perno, C.F.; Karlsson, A.; Balzarini, J.; Camarasa, M.J. 1,2,3-Triazole-[2,5-Bis-O-(tert-butyldimethylsilyl)-.beta.-D-ribofuranosyl]-3′-spiro-5″-(4″-amino-1″,2″-oxathiole 2″,2″-dioxide) (TSAO) Analogs: Synthesis and Anti-HIV-1 Activity. *J. Med. Chem.* **1994**, *37*, 4185–4194. [CrossRef]

14. De Clercq, E. In search of a selective antiviral chemotherapy. *Clin. Microbiol. Rev.* **1997**, *10*, 674–693. [CrossRef]

15. De Clercq, E. Strategies in the design of antiviral drugs. *Nat. Rev. Drug Discov.* **2002**, *1*, 13–25. [CrossRef]

16. De Simone, R.; Chini, M.G.; Bruno, I.; Riccio, R.; Mueller, D.; Werz, O.; Bifulco, G. Structure-Based Discovery of Inhibitors of Microsomal Prostaglandin E2 Synthase−1, 5-Lipoxygenase and 5-Lipoxygenase-Activating Protein: Promising Hits for the Development of New Anti-inflammatory Agents. *J. Med. Chem.* **2011**, *54*, 1565–1575. [CrossRef]

17. Guangyou, C.; Yiwan, Z.; Chonglin, C.; Jia, L.; Xing, Z. Synthesis and Antifungal Activity of Benzamidine Derivatives. *Molecules* **2014**, *19*, 5674–5691.

18. Costa, M.S.; Boechat, N.; Rangel, E.A.; Silva, F.D.C.D.; Souza, A.M.T.D.; Rodrigues, C.R.; Castro, H.C.; Junior, I.N.; Lourenc, M.C.S.; Wardell, S.M.S.V.; et al. Synthesis, tuberculosis inhibitory activity, and SAR study of N-substituted-phenyl- 1,2,3- triazole derivatives. *Bioorg Med. Chem.* **2006**, *14*, 8644–8653. [CrossRef]

19. Patpi, S.R.; Pulipati, L.; Yogeeswari, P.; Sriram, D.; Jain, N.; Sridhar, B.; Murthy, R.; Anjana, D.T.; Kalivendi, S.V.; Kantevar, S. Design, Synthesis, and Structure–Activity Correlations of Novel Dibenzo[b,d]furan, Dibenzo[b,d]thiophene, and N-Methylcarbazole Clubbed 1,2,3-Triazoles as Potent Inhibitors of Mycobacterium tuberculosis. *J. Med. Chem.* **2012**, *55*, 3911–3922. [CrossRef]

20. Genin, M.J.; Allwine, D.A.; Anderson, D.J.; Barbachyn, M.R.; Emmert, D.E.; Garmon, S.A.; Graber, D.R.; Grega, K.C.; Hester, J.B.; Hutchinson, D.K.; et al. Substituent effects on the antibacterial activity of nitrogen-carbon-linked (azolylphenyl)oxazolidinones with expanded activity against the fastidious gram-negative organisms Haemophilus influenzae and Moraxella catarrhalis. *J. Med. Chem.* **2000**, *43*, 953–970. [CrossRef]

21. De Las Heras, F.G.; Alonso, R.; Alonso, G. Alkylating nucleosides 1. Synthesis and cytostatic activity of N-glycosyl (halomethyl)-1,2,3-triazoles. A new type of alkylating agent. *J. Med. Chem.* **1979**, *22*, 496–500. [CrossRef]

22. Ouahrouch, A.; Ighachane, H.; Taourirte, M.; Engels, J.W.; Sedra, M.H.; Lazrek, H.B. Benzimidazole–1,2,3-triazole Hybrid Molecules: Synthesis and Evaluation for Antibacterial/Antifungal Activity. *Arch. Pharm. Chem. Life Sci.* **2014**, *347*, 748–755. [CrossRef]

23. Harkala, K.J.; Eppakayala, L.; Maringanti, T.C. Synthesis and biological evaluation of benzimidazole-linked 1,2,3-triazole congeners as agents. *Organic Med. Chem. Lett.* **2014**, *4*, 4–14. [CrossRef]

24. Mahdavi, M.; Ashtari, A.; Khoshneviszadeh, M.; Ranjbar, S.; Dehghani, A.; Akbarzadeh, T.; Saeedi, M. Synthesis of New Benzimidazole–1,2,3-triazole Hybrids as Tyrosinase Inhibitors. *Chem. Biodivers.* **2018**, *15*, e1800120. [CrossRef]

25. Pokhodylo, N.T.; Matiychuk, V.S.; Obushak, M.D. Synthesis of [1,2,3]triazolo-[4′,5′:4,5] pyrimido[1,6-a]benzimidazole, a new heterocyclic system. *Chem. Heterocycl. Comp.* **2009**, *45*, 245–247. [CrossRef]

26. Zefirov, Y.V.; Zorky, P.M. New applications of van der Waals radii in chemistry. *Russ. Chem. Rev.* **1995**, *64*, 415–428. [CrossRef]

27. Kitaigorodskii, A.I. *Organic Chemical Crystallography*; Consultants Bureau: New York, NY, USA, 1961.

28. Gillespie, R.J.; Popelier, P.L.A. *Chemical Bonding and Molecular Geometry*; Claredon Press: Oxford, UK, 2001.

29. Bernstein, J.; Davis, R.E.; Shimoni, L.; Chang, N.-L. Patterns in Hydrogen Bonding: Functionality and Graph Set Analysis in Crystals. *Angew. Chem. Int. Ed. Engl.* **1995**, *34*, 1555–1573. [CrossRef]

30. Etter, M.C. Encoding and decoding hydrogen-bond patterns of organic compounds. *Acc. Chem. Res.* **1990**, *23*, 120–126. [CrossRef]

31. Desiraju, G.R. *Crystal Design: Structure and Function Perspectives in Supramolecular Chemistry*; Wiley: Chichester, UK, 2003; Volume 7.

32. Desiraju, G.R. Supramolecular Synthons in Crystal Engineering—A New Organic Synthesis. *Angew. Chem. Int. Ed. Engl.* **1995**, *34*, 2311–2327. [CrossRef]

33. Desiraju, G.R. Chemistry beyond the molecule. *Nature* **2001**, *412*, 397–400. [CrossRef]

34. Shishkina, S.V.; Konovalova, I.S.; Shishkin, O.V.; Boyko, A.N. Acceptor properties of aminogroups in aminobenzene crystals: Study from the energetic viewpoint. *CrystEngComm* **2017**, *19*, 6274–6288. [CrossRef]

35. Shishkina, S.V.; Konovalova, I.S.; Shishkin, O.V.; Boyko, A.N. Influence of substituents on the acceptor properties of the amino groups in the diaminobenzene analogues. *CrystEngComm* **2017**, *19*, 7162–7176. [CrossRef]

36. Shishkin, O.V.; Dyakonenko, V.V.; Maleev, A.V. Supramolecular architecture of crystals of fused hydrocarbonsbased on topology of intermolecular interactions. *CrystEngComm* **2012**, *14*, 1795–1804. [CrossRef]

37. Shishkin, O.V.; Zubatyuk, R.I.; Maleev, A.V.; Boese, R. Investigation of topology of intermolecular interactions in the benzene–acetylene co-crystal by different theoretical methods. *Struct. Chem.* **2014**, *25*, 1547–1552. [CrossRef]

38. Endres, D.; Miyahara, M.; Moisant, P.; Zlotnick, A. A reaction landscape identifies the intermediates critical for self-assembly of virus capsids and other polyhedral structures. *Protein Sci.* **2005**, *14*, 1518–1525. [CrossRef]

39. Stray, S.J.; Zlotnick, A. BAY 41-4109 has multiple effects on Hepatitis B virus capsid assembly. *J. Mol. Recognit.* **2006**, *19*, 542–548. [CrossRef]

40. Choi, I.G.; Yu, Y.G. Interaction and assembly of HBV structural proteins: Novel target sites of anti-HBV agents. *Infect. Disord. Drug Targets* **2007**, *7*, 251–256. [CrossRef]

41. Wolber, G.; Langer, T. LigandScout: 3-D Pharmacophores Derived from Protein-Bound Ligands and Their Use as Virtual Screening Filters. *J. Chem. Inf. Model.* **2005**, *45*, 160–169. Available online: http://www.inteligand.com/ligandscout/ (accessed on 24 July 2019). [CrossRef]

42. Guo, H.; Cuconati, A. (Eds.) *Hepatitis B Virus: Methods and Protocols, Methods in Molecular Biology, V. 1540*; Springer Science+Business Media LLC: Berlin, Germany, 2017. [CrossRef]

43. Ivashchenko, A.V.; Mitkin, O.D.; Kravchenko, D.V.; Kuznetsova, I.V.; Kovalenko, S.M.; Bunyatyan, N.D.; Langer, T. Synthesis, X-Ray Crystal Structure, Hirshfeld Surface Analysis, and Molecular Docking Study of Novel Hepatitis B (HBV) Inhibitor: 8-Fluoro-5-(4-fluorobenzyl)-3-(2-methoxybenzyl)-3,5-dihydro-4H-pyrimido[5,4-b]indol-4-one. *Crystals* **2019**, *9*, 379. [CrossRef]

44. Donkers, J.M.; Zehnder, B.; van Westen, G.J.P.; Kwakkenbos, M.J.; Jzerman, A.P.; Oude Elferink, R.P.J.; Beuers, U.; Urban, S.; van de Graaf, F.J. Reduced hepatitis B and D viral entry using clinically applied drugs as novel inhibitors of the bile acid transporter NTCP. *Sci. Rep.* **2017**, *7*, 15307–15319. [CrossRef]

45. Sheldrick, G.M. SHELXT—Integrated space-group and crystal-structure determination. *Acta Cryst.* **2015**, *A71*, 3–8.

46. Macrae, C.F.; Bruno, I.J.; Chisholm, J.A.; Edgington, P.R.; McCabe, P.; Pidcock, E.; Rodriquez-Monge, L.; Taylor, R.; van de Streek, J.; Wood, P.A. Mercury CSD 2.0—New features for the visualization and investigation of crystal structures. *J. Appl. Crystallogr.* **2008**, *41*, 466–470.

47. Coppens, P. The use of a polarized hydrogen atom in X-ray structure refinement. *Acta Crystallogr. Sect. B Struct. Crystallogr. Cryst. Chem.* **1972**, *B28*, 1638–1640. [CrossRef]

48. Boys, S.F.; Bernardi, F. The calculation of small molecular interactions by the differences of separate total energies. Some procedures with reduced errors. *Mol. Phys.* **1970**, *19*, 553–566. [CrossRef]

49. Kendall, R.A.; Dunning, T.H., Jr.; Harrison, R.J. Electron affinities of the first-row atoms revisited. Systematic basis sets and wave functions. *J. Chem. Phys.* **1992**, *96*, 6796–6806.

50. Goerigk, L.; Grimme, S. A thorough benchmark of density functional methods for general main group thermochemistry, kinetics, and noncovalent interactions. *Phys. Chem. Chem. Phys.* **2011**, *13*, 6670–6688. [CrossRef] [PubMed]

51. Neese, F. *ORCA 2.8.0*; Universitaet Bonn: Bonn, Germany, 2010.